Uukuniemi virus infection causes a pervasive remodelling of the RNA-binding proteome in tick cell cultures

Alexandra Wilson[1,2#], Wael Kamel[1#], Kelsey Davies[1], Lesley Bell-Sakyi[3], Douglas Lamont[4], Yana Demyanenko[5], Eduardo Kitano[5], Marko Noerenberg[1], Alain Kohl[1,7], Shabaz Mohammed[5,6], Alfredo Castello[1]* & Benjamin Brennan[1]*

1. Medical Research Council–University of Glasgow Centre for Virus Research, Glasgow G61 1QH, Scotland, UK.
2. Veterinary Research Institute, Emerging Viral Diseases, Brno CZ-62100, Czech Republic; Department of Experimental Biology, Faculty of Science, Masaryk University, CZ-62500 Brno, Czech Republic; Institute of Parasitology, Biology Centre of the Czech Academy of Sciences, CZ-37005 Ceske Budejovice, Czech Republic
3. Institute of Infection, Veterinary and Ecological Sciences, University of Liverpool, Liverpool, L3 5RF, UK.
4. FingerPrints Proteomics Facility, School of Life Sciences, University of Dundee, Dundee, DD1 5EH, Scotland, UK
5. Rosalind Franklin Institute, Harwell Science and Innovation Campus, Oxfordshire, UK
6. Department of Chemistry, University of Oxford, Oxford, UK
7. Liverpool School of Tropical Medicine, Departments of Tropical Disease Biology and Vector Biology, Liverpool, UK.

[#], joint first authors

*, Correspondence: ben.brennan@glasgow.ac.uk; alfredo.castello@glasgow.ac.uk

ORCID:

Alexandra Wilson	0000-0003-3328-1462
Wael Kamel	0000-0002-7625-2648
Kelsey Davies	0009-0009-5624-5983
Lesley Bell-Sakyi	0000-0002-7305-0477
Douglas Lamont	0000-0002-2262-5680
Yana Demyanenko	0000-0002-6628-1912
Eduardo Kitano	0000-0002-5718-7510
Marko Noerenberg	0000-0002-4834-8888
Alain Kohl	0000-0002-1523-9458
Shabaz Mohammed	0000-0003-2640-9560
Alfredo Castello	0000-0002-1499-4662
Benjamin Brennan	0000-0003-4707-726X

Keywords:

Bunyavirus, Uukuniemi virus, tick cell, RNA binding proteome, RNA-binding protein, protein-RNA interaction, RNA, host-virus interactions

Abstract

RNA-binding proteins (RBPs) are pivotal for the viral lifecycle, mediating key host-virus interactions that promote or repress virus infection. While these interactions have been largely studied in the vertebrate host, no comprehensive analyses of protein-RNA interactions occurring in cells derived from the infected vector have been done to date, particularly for ticks. Here we systematically identify the responses of the RNA-binding proteome (RBPome) to infection with a prototype bunyavirus (Uukuniemi virus; rUUKV) in tick cells and discovered changes in RNA-binding activity for 283 proteins. In an orthogonal approach, we analysed the interactions of the viral ribonucleoprotein by immunoprecipitation of UUKV nucleocapsid (NCAP) in infected cells. We found that tick cell derived RBPs are regulated by UUKV and associate with N complexes, suggesting a functional connection with infection. We confirmed experimentally that these RBPs impact UUKV infection, with TOP3B showing a putative effect on viral particle production. Our data thus reveals the first protein-RNA interaction map determined in infected tick cells.

Research highlights

- UUKV RNAs interact with nearly three hundred tick cell RBPs
- We found an enrichment of NCAP interactors within the upregulated RIC data suggesting a direct involvement in viral RNA processing
- Developed a robust methodology to silence gene expression in tick cell cultures
- The TOP3B complex facilitates efficient packaging of UUKV virions.

INTRODUCTION

Uukuvirus uukuniemiense is the type species within the genus *Uukuvirus* of the family *Phenuiviridae* that was first isolated from *Ixodes ricinus* ticks in Finland in 1964 [1]. Uukuniemi virus (UUKV; strain S-23) has been utilised as the prototype tickborne bunyavirus for several decades and has contributed to many aspects of bunyavirus research [2,3], such as the determination of the tri-segmented nature of bunyaviruses [4], the isolation of the first RNA-dependent RNA polymerase from a bunyavirus [5], the determination of the structural composition of the virion [6] and entry into mammalian cells [7-9]. Like other phenuiviruses, the genome of UUKV is comprised of three segments of negative or ambi-sense RNA, named small (S), medium (M) and large (L) present in the cytoplasm of infected cells as ribonucleoprotein complexes with the viral nucleocapsid (N) protein and RNA-dependent RNA polymerase (L protein) [10]. The virus also encodes a non-structural protein (NSs) within the S segment that has been demonstrated to be a weak interferon antagonist [11]. However, unlike other phenuiviruses transmitted by mosquitoes or sandflies, the M segment of tickborne phenuiviruses only encode the glycoprotein precursor and do not encode for any other non-structural proteins [12].

Research into tickborne bunyaviruses has been heavily biased towards studies in vertebrate systems, primarily due to the difficulty of culture and lack of genomic data or molecular reagents to conduct virus infection experiments within tick-derived cell lines. To date, over 70 cell lines have been developed from different and diverse tick species [13]. While only within the last 10 years has detailed tick genome data from

95 whole ticks been published by several groups [14,15] and the draft genome of one tick
96 cell line derived from *Ixodes scapularis* [16]. These tools have facilitated several
97 groups to conduct whole cell and immunoprecipitation proteomics, transcriptomic and
98 genomic analysis of tick-derived cell lines have already been undertaken by several
99 groups [17-25]. However, no research has been carried out to determine the host
100 proteins with pivotal roles in the lifecycle of a bunyavirus within tick cells.
101
102 RNA viruses have a limited coding capacity, and therefore cannot encode all
103 the proteins required for a fully autonomous lifecycle. For example, viruses rely on the
104 translation apparatus of the host cell to synthesise viral proteins, with the ribosome
105 being composed by over 80 proteins and several ribosomal (r)RNAs. However, protein
106 synthesis is one of the steps of virus infection and other cellular RBPs are expected
107 to participate in RNA stability, replication and packaging within the viral particles [26].
108 RBPs are also critical in the cellar defence against viruses, and in vertebrates, virus
109 sensors and effectors recognise molecular patterns that are specific to viral RNAs. In
110 invertebrates, it is believed the RNAi pathway, which utilises many RBPs such as
111 DICER and AGO, are the main effectors of the antiviral response. Despite the central
112 roles that RNA plays in the viral lifecycle, the catalogue of host RBPs that participate
113 in viral infection remains largely unknown, particularly for vector models such as ticks
114 [27-30].
115
116 In this manuscript, we utilise our proteome-wide approach called RNA
117 interactome capture (RIC) to study the responses of the tick RNA-binding proteome
118 (RBPome) to the infection with rUUKV. This work builds on our utilisation of the RIC
119 approach to identify the complement of RBPs in a range of arthropod cells (manuscript
120 in preparation) including the *Ixodes scapularis* derived cell line, ISE6 [31]. We
121 discovered that the tick RBPome is has great plasticity and varies throughout infection,
122 with over two hundred proteins exhibiting either an increased or decreased RNA-
123 binding activity. In addition, we conducted an orthogonal approach to isolate the viral
124 ribonucleoproteins (RNP) via immunoprecipitation of the UUKV N protein. Strikingly,
125 we found that 18 RBPs with virus-regulated RNA-binding activity are associated with
126 the viral ribonucleoproteins. We validated our findings with dsRNA knockdowns in
127 ISE6 cell cultures showing that the discovered RBPs do regulate virus infection. Initial
128 characterisation of the selected candidates revealed a role for the protein *ISCI010954*
129 (*TOP3B* in mammals) in the production of infectious virus particles.
130

131 RESULTS

132 Establishing comparative RNA interactome capture (cRIC) in tick cells

133 Our goal is to determine how virus infection alters the landscape of RBPs in
134 virus infection [28,29,32]. In a first step, we determined the optimal conditions to
135 perform RNA Interactome Capture (RIC) on a tick cell line derived from *I. scapularis*,
136 ISE6 [manuscript in preparation]. We then used the established conditions to perform
137 a comparative experiment between uninfected and rUUKV-infected cells (Fig 1A). To
138 determine which timepoint to utilise for this analysis we conducted a viral growth curve
139 to examine rUUKV infection kinetics within the tick cell line. Release of infectious virus
140 into the cell culture supernatant was detected throughout the course of infection and
141 progressively increased until the final time point at 12 days p.i. (Fig 1B). In parallel,
142 expression of the viral nucleocapsid protein was monitored in infected cell monolayers
143 derived from the virus growth curve. UUKV N protein was only detectable by Western

blotting analysis from 9 days p.i. (Fig 1C). Based on these findings 9 days p.i, was selected to maximise the probability of the cells in the monolayer being infected and a time at which viral RNA is exponentially replicating within the infected cell. rUUKV-infected cell monolayers were also analysed by confocal microscopy through staining the monolayer for the presence of the UUKV N protein. This qualitative assessment provided assurance that most cells were infected at this timepoint and confirmed its suitability for cRIC analysis (Fig 1D).

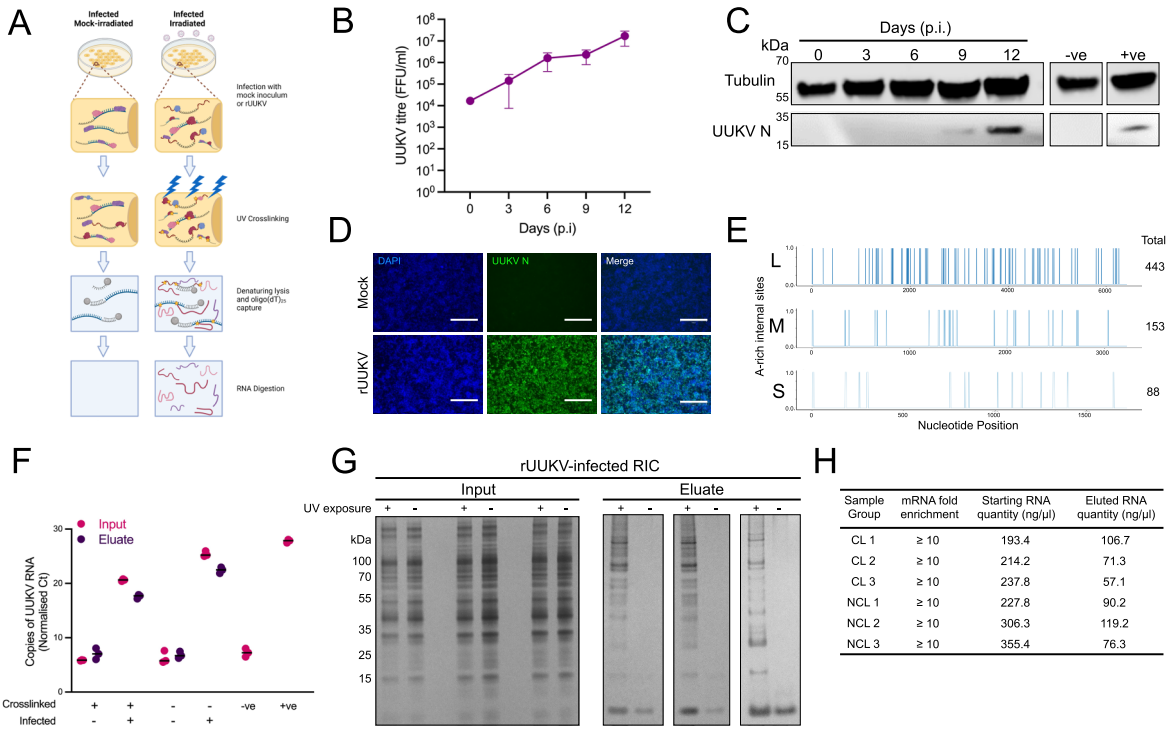

Sample Group	mRNA fold enrichment	Starting RNA quantity (ng/µl)	Eluted RNA quantity (ng/µl)
CL 1	≥ 10	193.4	106.7
CL 2	≥ 10	214.2	71.3
CL 3	≥ 10	237.8	57.1
NCL 1	≥ 10	227.8	90.2
NCL 2	≥ 10	306.3	119.2
NCL 3	≥ 10	355.4	76.3

Fig 1. Preparation of mock and rUUKV-infected RNA interactome capture (RIC) samples derived from ISE6 cell cultures.

Infection conditions for cell cultures derived from the tick *Ixodes scapularis* (ISE6) were established, and preparations of mock or rUUKV-infected ISE6 cell monolayers were harvested at 9 days p.i. (in triplicate) were exposed to 150mJ/cm^2 or mock-irradiated before lysis and interactome capture.

(A) Schematic showing the methodology of interactome capture utilising UV-crosslinking and oligo(dT)$_{25}$ capture beads.

(B) ISE6 cell cultures were infected with rUUKV at an MOI of 5 FFU/cell. At the indicated time p.i., culture supernatants were collected for virus titration by immunofocus assay on BSR cells. Data are plotted as the mean virus titre (FFU/ml) ± SD of n=3 biological replicates.

(C) Cell extracts from the rUUKV infected cell monolayers which produced the titration results in (B) were prepared to analyse viral protein expression. Western blots were probed with anti-α tubulin, and anti-UUKV N antibodies as indicated in the representative image. '-ve': mock-infected cell lysate; '+ve': sample known to be infected with rUUKV derived from mammalian cell infections.

(D) ISE6 cell monolayers were infected with rUUKV at a MOI of 5 FFU/cell or mock infected. At 9 days p.i., ISE6 cell monolayers were fixed, stained with DAPI (blue), and probed for UUKV N protein (green) to qualitatively investigate the percentage infection of the cell monolayers. Cell monolayers were imaged using an EVOS microscope using a 10x lens. Scale bar is equal to 300 µm.

(E) A poly(A) adjacent scan was run on each of the UUKV RNA genome segments, with poly(A)/poly(A)-like being defined as a minimum of 5 continuous A nucleotides and any larger sections being at least 80% A content. The involvement of each nucleotide in poly(A)/poly(A)-like site are visualized.

(F) Samples of rUUKV-infected ISE6 cell monolayers harvest at 9 days p.i. were prepared and RT qPCR analysis was conducted on these samples using UUKV M oligos. RNA isolated from non-infected ISE6 cells was used as a negative control, and RNA from rUUKV-infected ISE6 cells sampled at 12 days p.i. were used as positive control. Ct values were normalized by subtracting the Ct of the sample from the

Ct limit of the system (Ct = 40), with the confidence cut-off for the presence of rUUKV being a normalized Ct of 10 as defined by blank RT qPCR results.
(G) rUUKV-infected ISE6 were harvested at 9 days p.i. and subjected to interactome capture in triplicate. Before RNA digestion, a small volume of each input and eluate sample was processed and protein digested to allow for RNA analysis. Input samples were extracted, and cell lysates were prepared for RNA interactome capture (RIC) using oligo(dT) capture beads, followed by RNA digestion for protein analysis. Samples were subjected to RNA digestion to allow for protein analysis, separated by SDS PAGE and resolved proteins were visualized using silver staining.
(H) RNA quantities in the cross-linked (CL) and non-cross-linked (NCL) input and elute samples of rUUKV-infected ISE6 cell cultures were measured via a nanodrop spectrophotometer. RT qPCR was performed against the 18S ribosomal RNA and eukaryotic elongation factor 1-alpha (*ELF1A*; mRNA used as a housekeeping gene) The ΔΔCT method was used to measure the quantity of 18S RNA normalized to *ELF1A* RNA levels, and the mRNA fold enrichment in the elute compared to the input sample was calculated for each biological sample.

During infection, the ratio of viral RNA to cellular mRNA increases as viral replication progresses and this can lead to interference cellular mRNA production. To obtain a complete picture of the intracellular environment during rUUKV infection of ISE6 cells, it was therefore important to ensure the capture of both cellular and viral RNA. This presents a problem, as bunyaviral genomic RNA or mRNAs are non-polyadenylated [33,34] and the oligo$(dT)_{25}$ capture beads used in cRIC exploit the interaction between the poly-A tail of mRNAs. We analysed the genome of UUKV for the presence of 'poly-A like' regions, which we defined as a minimum of five sequential A nucleotides and any larger region containing a ≥80% A content. Our hypothesis was that oligo$(dT)_{25}$ capture beads would be able to capture the UUKV RNA by interacting with these 'poly-A like' regions, allowing the interactome capture to reflect both viral and cellular RNA within the infected cells. Our *in-silico* analysis revealed 88, 153 or 443 poly-A-like regions present within the UUKV S, M or L RNAs, respectively (Fig 1E). These results provided a basis for continuing with the rUUKV-infected cRIC experimental protocol.

We performed the cRIC in triplicate for both mock- or rUUKV- infected ISE6 cell cultures, with corresponding mock-irradiated samples as a control. Before RNA digestion, an aliquot of each sample was taken and subjected to protein digestion to isolate total RNA and the presence of UUKV RNA within the input or eluate samples was determined by qPCR targeting a region of the UUKV M segment. UUKV M RNA was detected in all infected samples, whilst the mock-infected samples remained negative (Fig 1F). These data confirmed that the oligo$(dT)_{25}$ capture beads could interact with viral RNA, regardless of if protein was cross-linked to the RNA and therefore demonstrated the rUUKV-infected eluate did reflect the composition of mRNAs present in the infected cells (Fig 1E & 1F). Samples were then subjected to RNA digestion to allow for downstream protein analysis. Silver staining of the input and eluate samples of the rUUKV infected samples (Fig 1G) were performed to visualise the isolated proteins, and corresponding RNA quantities were measured using Nanodrop One (Fig 1H). No proteins were detected within the mock-irradiated samples, and the change in banding patterns between the input and elute indicates that a subsection of the whole cell proteome was isolated, confirming this technique was suitable for RBPome capture. The irradiated samples were then sent for mass spectrometry analysis. The determination of the tick cell RBPome was conducted in our previous studies [manuscript in preparation]. Here, we present mass spectrometry results of the rUUKV-infected samples, to allow for comparison of the tick cell RBPome between mock- and rUUKV-infected state, thereby determining the first differential RBPome of virus infected tick cell cultures.

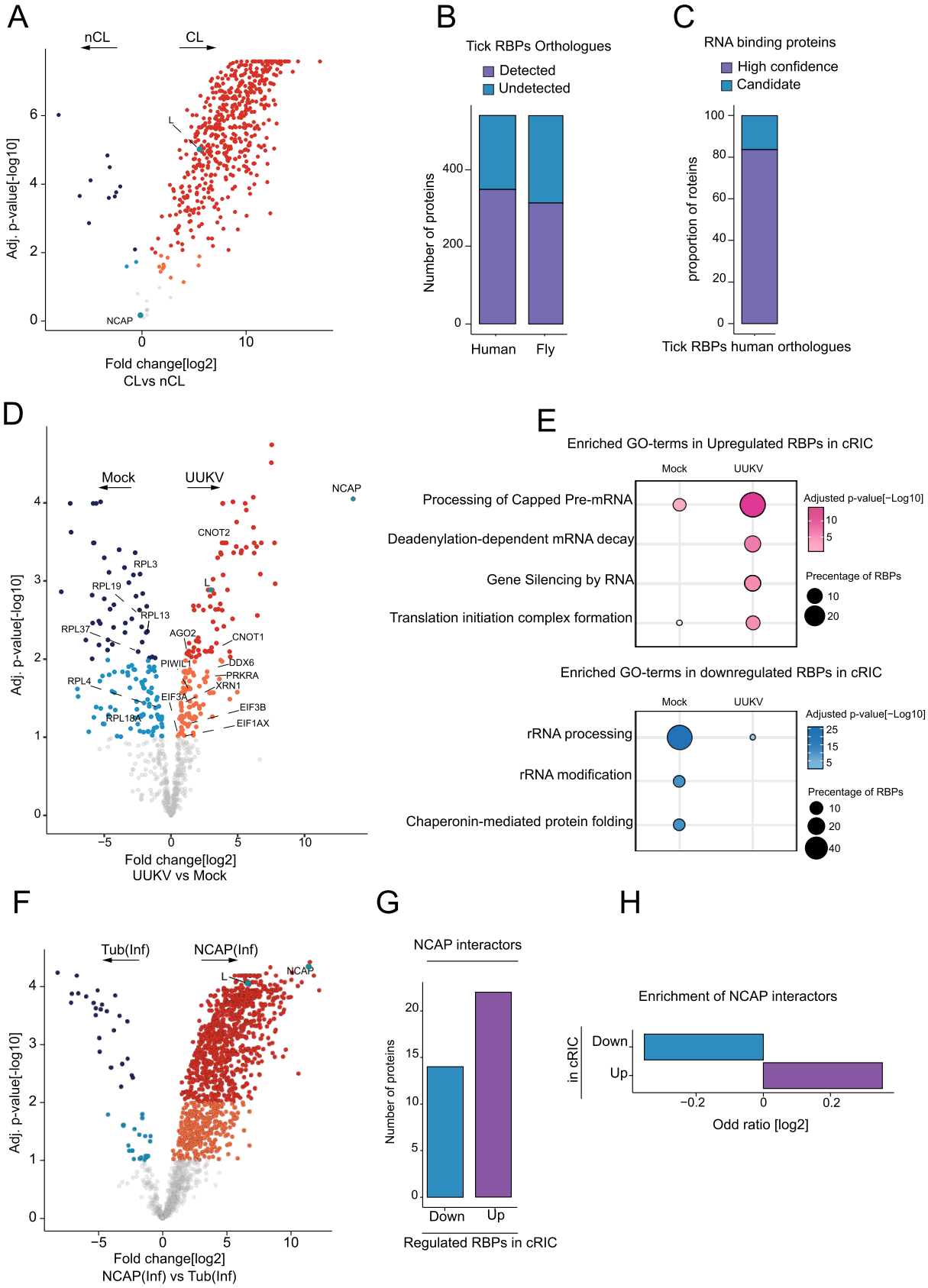

Fig 2. Differential regulation of RBPome during UUKV- infection in ISE6 cells.
(A) The fold change in the proteins found in the UUKV-infected cross-linked samples compared to the non-cross-linked (x-axis) were plotted against the significance of this fold change (Adj. p value[-log10], y axis). For proteins with a positive fold change, proteins at a 1-10% false discovery rate are coloured

in orange and proteins at a 1% false discovery rate or below are coloured red. For proteins with a negative fold change, proteins at a 1% false discovery rate or below are coloured dark blue.
(B) InParanoid analysis was performed to determine the number of proteins which had corresponding human and drosophila orthologs (purple) within the differential RBPome.
(C) The human orthologs identified in (B) were compared against a defined experimentally proven database of RNA binding proteins (RBPbase v0.2.1 alpha). Proteins which were found by three independent studies were termed high confidence (purple), while the other proteins were termed candidates.
(D) The fold change in the proteins of the rUUKV-infected cross-linked samples were compared to the mock cross-linked samples (x axis) were plotted against the significance of this fold change (Adj. p value[-log10], y axis). For proteins with a positive fold change, proteins at a 1-10% false discovery rate) are coloured in orange and proteins at a 1% false discovery rate or below are coloured red. For proteins with a negative fold change, and therefore in higher quantities in non-cross-linked samples, proteins at a 1-10% FDR coloured in light blue, and proteins at a 1% FDR or below are coloured dark blue. Proteins with greater than 10% FDR are shown in grey**.**
(E) Enrichment of cellular pathways in the upregulated (shown in pink) and downregulated (shown in pink) RNA binding proteins in the cRIC during UUKV- infection.
(F) Fold change of proteins found in the rUUKV-infected samples using UUKV N or tubulin antibody immunoprecipitation were compared.
(G) The number of differentially regulated RBPs in cRIC interacting with NCAP.
(H) The odds ratio of the NCAP interactors found in the upregulated and downregulated RIC RBPs were calculated to determine the enrichment of the NCAP interactors in the RIC data.

Differential RNA binding and regulation of cellular pathways during rUUKV infection.

Diagnostic analysis was performed on the mock and rUUKV-infected mass spectrometry outputs (Fig S1). The distribution of proteins intensities between the biological triplicates of all samples showed minimal variation, with the cross-linked samples displaying a greater intensity than the non-cross-linked counterparts (Fig S1A). Principal Component Analysis (PCA) was used to examine the variability between our cRIC samples. The data demonstrated that all triplicate samples from each of the respective conditions grouped discretely together. The factor that accounted for the largest proportion of the variability (~85%) was whether the samples were subjected to UV radiation and the second variable (~6%) was determined to be if the samples were infected with rUUKV (Fig S1B). From these results it was established data could be used for further analyses to characterise the infected ISE6 RBPome.

Within the rUUKV-infected sample dataset, we identified 572 proteins, of which 541 and 530 proteins were present at a false discovery rate (FDR) of 10% and 1%, respectively (Fig 2A). Due to the lack of information and annotation within the genome of the ISE6 cell line, we chose to include all proteins identified in the 10% FDR groups to maximise the output from the results, this group was identified as the 'rUUKV-infected cell RBPome'. Using the proteins sequences identified in the rUUKV-infected cell RBPome, we identified the number of corresponding orthologous human *(Homo sapiens*) and fly *(Drosophila*) proteins using InParanoid analysis [37]. Approximately 65% and 58% of the differential RBPome was identified to have a human or fly orthologs, respectively (Fig. 2B). Of these 349 proteins which were found to have corresponding human orthologs, over 80% of these orthologs have been experimentally proved to have RNA binding capabilities (Fig. 2C). Therefore, we concluded this interactome consisted of RNA binding proteins and was suitable for establishment of a differential RBPome by direct comparison to the ISE6 mock-infected RBPome.

289 In the comparison between mock versus UUKV-infected UV-crosslinked
290 samples, we identified 283 differentially regulated RNA binding proteins in the 10%
291 FDR group (Fig. 2D). Reassuringly, both the viral nucleocapsid protein (NCAP) and
292 RNA-dependent RNA polymerase (L) were identified as significantly up regulated in
293 rUUKV-infected cells compared to mock-infected samples.
294 Cellular pathways enrichment analysis for proteins with altered RNA binding activity
295 revealed pronounced changes happening during UUKV-infection (Fig. 2E). Among the
296 enriched pathways in the upregulated RBPs in cRIC, those involved in RNA
297 processing and translation initiation that are potentially involved in viral RNA and
298 proteins production. Also, pathways involved in mRNA decay and RNAi-mediated
299 gene silencing that could be reflecting host-virus interactions, targeting viral RNA or
300 specific cellular RNA for degradation. Interestingly, ribosomal proteins formed most
301 downregulated RNA binding proteins during UUKV infection.
302

303 **Elucidating UUKV N protein-specific interactors and comparison of cellular**
304 **proteins identified in cRIC and IP datasets.**

305 As bunyaviral RNAs are found strongly associated with the viral nucleoprotein
306 which encapsidates the viral ribonucleoprotein (RNP) complexes present in the
307 cellular cytoplasm, we next investigated which ISE6 proteins interacted with the N
308 protein rather than the viral RNA during rUUKV infection. This was performed in mock-
309 or rUUKV-infected ISE6 cells harvested at 9 days p.i., at which time samples were
310 immunoprecipitated with either an anti-N or anti-tubulin antibody to elucidate the
311 interacting partners and to allow comparative analysis with the cRIC data obtained.
312 Diagnostic analysis was performed on the mass spectrometry results of the I.P.
313 experiment (Fig S1). The data show discrete clustering of triplicate samples with
314 87.4% of the variance explained by infection status and 7.1% of the variance explained
315 by which antibody was used for the immunoprecipitation (IP) (Fig S1C).
316 When comparing the proteins isolated by anti-tubulin antibody compared to anti-UUKV
317 N antibody in infected cells, we identified 922 at FDR 10%, of which 701 proteins were
318 present in the 1% FDR group (Fig 2F). In addition, we compared the proteins isolated
319 by anti-UUKV N antibody in infected cells and mock-infected cells, where 613 proteins
320 were present at an FDR of 10% (Fig. S1D). Similar to the RIC data, both the viral
321 nucleocapsid protein (NCAP) and RNA-dependent RNA polymerase (L) were
322 identified as significantly up regulated in rUUKV-infected cells compared to mock-
323 infected samples and within N pulldown cells compared to tubulin pulldown in infected
324 cells. For more stringent analysis, we cross-referenced the 10% FDR groups of the
325 infected cell tubulin vs UUKV N protein pulldown (Fig. 2F) and mock infected vs UUKV
326 infected UUKV N pulldown (Fig. S1D). A total of 378 proteins were found to be present
327 in both groups (Fig. S1E), and the proteins within the 10% FDR groups of both these
328 analyses were assigned NCAP interactors.
329 We cross-referenced the NCAP interactors with our previously generated differential
330 RBPome (defined in Fig 2D). Of the 378 proteins immunoprecipitated from rUUKV-
331 infected cells, 14 and 22 proteins were found within the downregulated and
332 upregulated differential RBP groups, respectively (Fig. 2G). Finally, the odds ratio of
333 the NCAP interactors found in the upregulated and downregulated RBPs (as
334 determined by RIC) were calculated to determine the enrichment of the NCAP
335 interactors in the RIC data (Fig. 2H). We found there was a modest enrichment of
336 NCAP interactors within the upregulated RIC data suggesting their direct involvement
337 in vRNA processing.

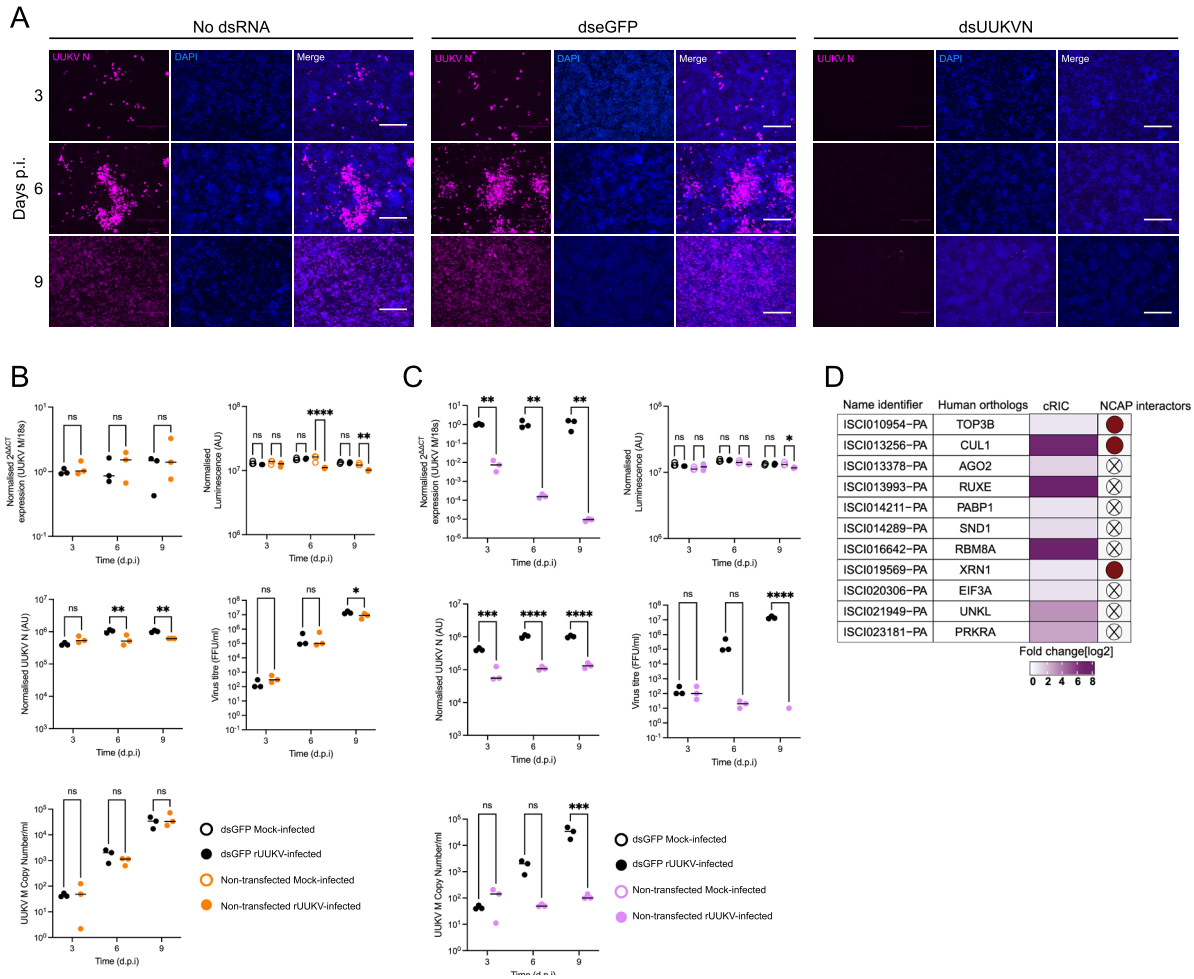

Fig 3. Effect of eGFP dsRNA or UUKV N dsRNA transfection on rUUKV replication in infected ISE6 cells.

To determine the impact of transfection and efficiency of dsRNA-mediated silencing in ISE6 cell cultures a pilot experiment was conducted. ISE6 cell monolayers were transfected with 2µg of either dsRNA to eGFP (dseGFP) or UUKV N (dsUUKV N) or mock-transfected. At 24 h p.t., cell monolayers were infected with rUUKV at 5 FFU/cell and harvested for analysis via immunofluorescence or RT-qPCR at the time points indicated.

(A) Fixed cell monolayers were harvested at each time point and permeabilised and stained using DAPI (blue) and mouse anti-UUKV N (green). Imaging was carried out using an EVOS microscope, scale bar 300 µm. In parallel, cell monolayers were lysed with TRIzol and RNA extracted at the timepoints indicated. For all RT qPCRs, primers against UUKV M and *I scapularis* ribosomal 18S were used. Each gene type knockdown biological replicate was carried out conjointly with all other gene type knockdowns alongside the positive and negative controls, therefore each individual gene knockdown was compared to the same positive and negative control carried out using this method.

(B) mock (black) vs dseGFP (orange) or **(C)** mock (black) vs dsUUKV N (pink) are shown. Parameters examined include quantity of intracellular UUKV M RNA (normalised $2^{\Delta\Delta CT}$), cell viability (normalised luminescence), UUKV N expression via in well western blot (normalised UUKV N), UUKV titre (FFU/ml) and UUKV M RNA (UUKV M RNA copy number/ml) present in cell culture supernatant.

(D) Eleven targets were selected for knockdown analysis, each having a corresponding human ortholog. The fold change within the cRIC data [log2] is indicated in purple as defined in Fig. 2D, alongside whether the protein is defined as an NCAP interactor as specified in Fig. 2G. Statistical significance was measured by ordinary two-way ANOVA with Tukey's multiple comparisons test. Asterisks indicates significance **** = $p < 0.0001$, *** = $p \leq 0.001$, ** = $p \leq 0.01$, * = $p \leq 0.05$, ns = not significant.

365 **dsRNA delivery into ISE6 cell cultures and selection of candidate RBPs for**
366 **dsRNA knockdown during rUUKV infection**

367 To begin evaluating the roles of the differentially active RBPs and their importance in
368 rUUKV-infection, we selected several targets for downstream double stranded (ds)
369 RNA knockdown. Firstly, we designed dsRNA controls to optimise the transfection
370 methodology and to assess the impact upon and efficiency of transfection of the ISE6
371 cell cultures (Fig 3). We utilised a previously optimised Magnetofection technology to
372 deliver dsRNA into tick cells [35]. ISE6 cells were either mock-transfected or
373 transfected with dsRNA targeting sequences derived from either eGFP or UUKV N
374 and subsequently infected with rUUKV. Varying parameters such as cell viability,
375 UUKV N protein expression (confocal microscopy quantification); intracellular virus
376 replication and the release of viral RNA into the supernatant, measured by RT-qPCR;
377 and release of infectious virions (IFA analysis) were studied at the time points
378 indicated. Confocal microscopy analysis of rUUKV-infected ISE6 monolayers showed
379 that there was robust UUKV infection over the time course in both the mock-
380 transfected and dseGFP transfected monolayers. In contrast, transfection of a dsRNA
381 targeting UUKV N almost completely abrogated UUKV infection (Fig 3A). This result
382 was further supported observing the tested parameters. No difference in UUKV
383 replication, N protein production, virion RNA in the supernatant or release of infectious
384 virus was observed in dseGFP-transfected monolayers (Fig 3B), but a significant
385 decrease in was observed when the dsRNA transfected targeted the UUKV N
386 sequence (Fig 3C). In both vases only small variations in cell viability were observed.
387 These data demonstrated that we could efficiently deliver dsRNA into tick cells robustly
388 and that that delivered dsRNAs could be utilised to silence genes within the tick cell
389 cultures.
390
391 Now that the differential RBPome has been elucidated, and the transfection method
392 was optimised, several targets were selected for further analysis as shown in Fig 3D.
393

394 **Effect of the depletion of RBPs on rUUKV replication in ISE6 cells.**

395 To assess the impact of the RBPs identified, ISE6 cells were transfected with either
396 dsRNA corresponding to the respective RBP mRNA or a dsRNA to eGFP as a control.
397 Following transfection cells were infected with rUUKV and harvested at the indicated
398 time points post infection. Most transcripts were effectively knocked down in
399 transfected cells receiving dsRNA to the cellular target. However, the knockdown
400 efficiency of *CUL1*, *PRKRA*, and *XRN1* at later timepoints was only approximately 50%
401 (Fig S2). No antibodies are currently available to confirm a reduction in protein
402 expression that target the ISE6 cellular proteins we have identified. Therefore, RT-
403 qPCR is currently the only reliable methodology to assess the gene silencing efficiency
404 in tick cells. We also examined the viability of each of the dsRNA knockdowns over
405 the time course of infection. Overall cell viability was maintained for most of the dsRNA
406 knockdowns, over all three timepoints. However, there was a reduction in cell viability
407 observed in rUUKV-infected samples compared to the uninfected controls at several
408 timepoints and a reduced cell viability observed at 9 d p.i. timepoints for the PABP1,
409 PRKRA and UNKL knockdowns (Fig S3).
410

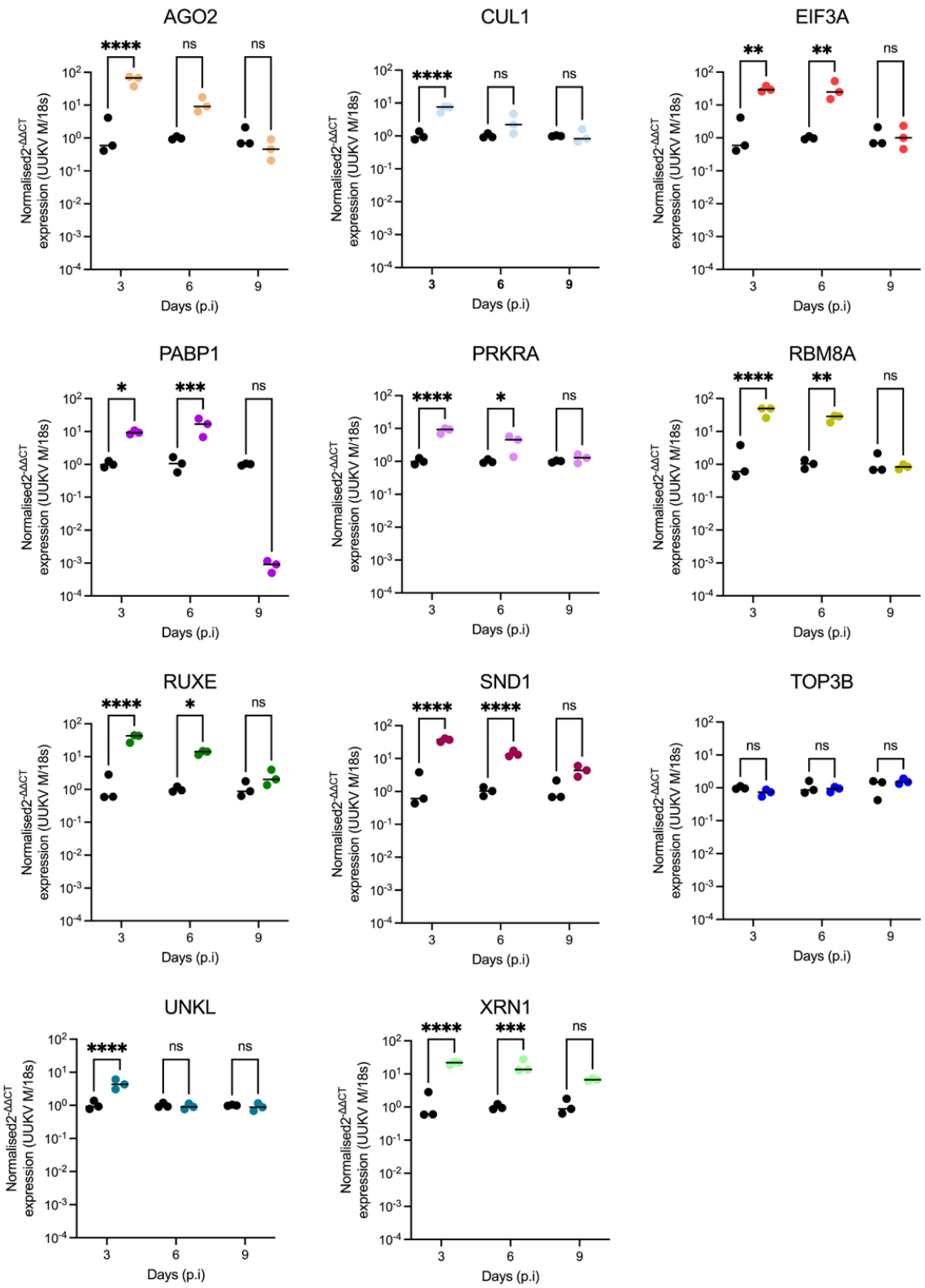

411
412 **Fig 4. Effect of dsRNA transfections on the expression of UUKV M RNA levels within UUKV**
413 **infected ISE6 cell culture.**
414 Triplicate ISE6 cell monolayers were transfected with 2µg of dsRNA homologous to the indicated gene.
415 Black symbols represent dseGFP data (mock) and coloured symbols represent dsGene data. At one
416 day post-transfection, cell monolayers were infected with rUUKV at 5 FFU/cell. At timepoints indicated,
417 cell monolayers were lysed via TRIzol and cellular RNA extracted. RT qPCR was performed on the
418 cellular RNA using primers against UUKV M RNA, and *I. scapularis* ribosomal 18S as the
419 'housekeeping' gene. The normalised expression of UUKV M RNA was calculated using the 2-ΔΔCt

method. Statistical significance was measured by ordinary two-way ANOVA with Tukey's multiple comparisons test. Asterisks indicates significance **** = $p < 0.0001$, *** = $p \leq 0.001$, ** = $p \leq 0.01$, * = $p \leq 0.05$, ns = not significant.

The amount of intracellular UUKV M RNA was quantified at each time point in both the ISE6 cells receiving the GFP or gene specific dsRNA. Many of the gene knockdowns resulted in a statistically significant increase in UUKV M RNA at either the 3- or 6-day time point (Fig 4). This is not unexpected considering the known antiviral roles of proteins such as Ago2 and XRN1 in other mammalian or arthropod systems. The knockdown of other genes involved in the translation of cellular mRNAs such as EIF3A and PABP1 also resulted in an increased accumulation of UUKV mRNA in the cell. Conversely, the knockdown of TOP3B within the ISE6 cells did not have any impact on the quantity of UUKV M RNA and hence virus replication at any of the time points indicated (Fig 4).

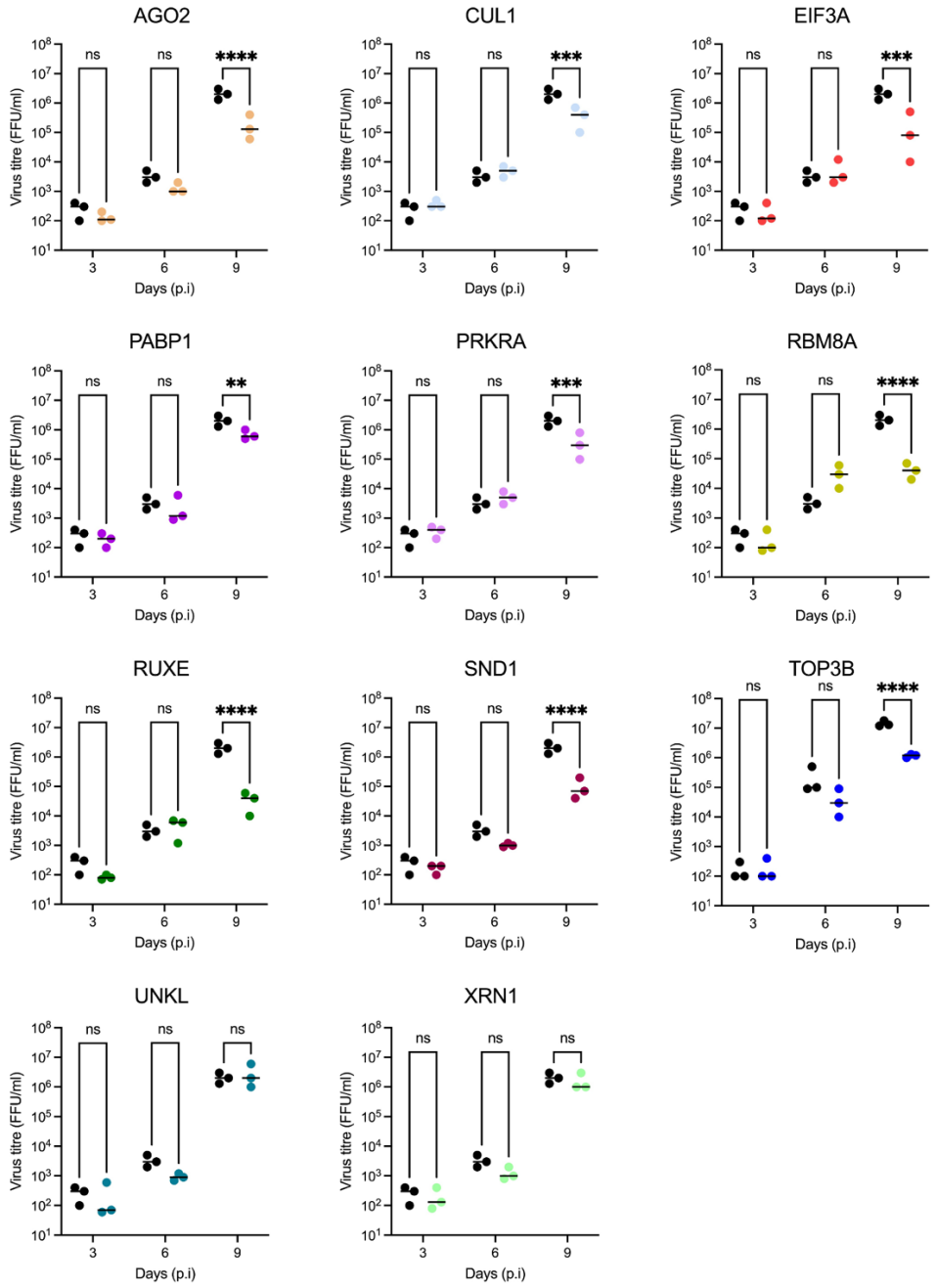

Fig 5. Effect of dsRNA transfections on UUKV supernatant titre within UUKV infected ISE6 cell cultures.
Triplicate ISE6 cell monolayers were transfected with 2µg of dsRNA homologous to the indicated gene. Black symbols represent dseGFP data (mock) and coloured symbols represent dsGene data. At one day post-transfection, cell monolayers were infected with rUUKV at 5 FFU/cell. At timepoints indicated, cell supernatant was harvested, and titres determined using foci-forming assay. Statistical significance was measured by ordinary two-way ANOVA with Tukey's multiple comparisons test. Asterisks indicates significance **** = $p < 0.0001$, *** = $p \leq 0.001$, ** = $p \leq 0.01$, * = $p \leq 0.05$, ns = not significant.

The release of both infectious virus particles (Fig 5) and the presence of viral RNA in the supernatant (Fig 6) were assessed over the infection time course. Only a small amount of infectious virus was detectable into the supernatant at 3 days p.i. (approx. 10^2 FFU/ml) in the dseGFP treated control. This increased over time to ~10^6 FFU/ml by 9 days p.i. Surprisingly, the increased detection of UUKV M RNA in the knockdown cells demonstrated in Fig 4 did not translate into an increase of infectious virus release at any of the time points tested. An observable and significant decrease in the production of infectious UUKV was observed at 9 days p.i. in all knockdown samples with the exception of UNKL and XRN1 where no significant difference was observed (Fig 5).

This decrease in UUKV titre is likely due to a reduction of cell viability of the knockdown cell producing the virus at 9 days p.i. (Fig S2). Assessing the difference in viral RNA release and supernatant titre provides a proxy measurement for the number of defective or non-infectious particles that have been produced from the infected tick cell. In the case of both UNKL and XRN1 knockdown, a decrease in the amount of viral RNA present in the supernatant was observed, despite no corresponding reduction in virus titre being recorded, suggesting that the knockdown of these genes may have increased the number of infective particles produced while slowing the rate of packaging of the viral RNA into the budding virion (Fig 5 & Fig 6).

Conversely, a decrease in infectious virus produced, but no parallel decrease in viral RNA detected in the supernatant was observed in the TOP3B knockdown. Indicating that although the same level of RNA was being released from the cells not all the viral particles that were released were infectious. This result was of particular interest as previous research has shown TOP3B knockout impairs the production of infectious *Flavivirus* particles, although overall release of virions was unaffected [36], as shown in our data with UUKV.

DISCUSSION

Research into arboviruses that are transmitted by ticks have largely focussed on the interactions the virus has with vertebrate cells and systems. A major contributing factor to the dearth of research into arthropod-virus interactions has been the lack of viable cell culture or *in vivo* systems. In recent years, a range of tick cell lines have been generated, curated and continually updated [37] and the genomes of both the *I. scapularis* tick [38] and derived ISE6 cell line [16] have been annotated. This has allowed research to begin to probe into how tickborne arboviruses manipulate the vector cell to facilitate their own replication and transmission.

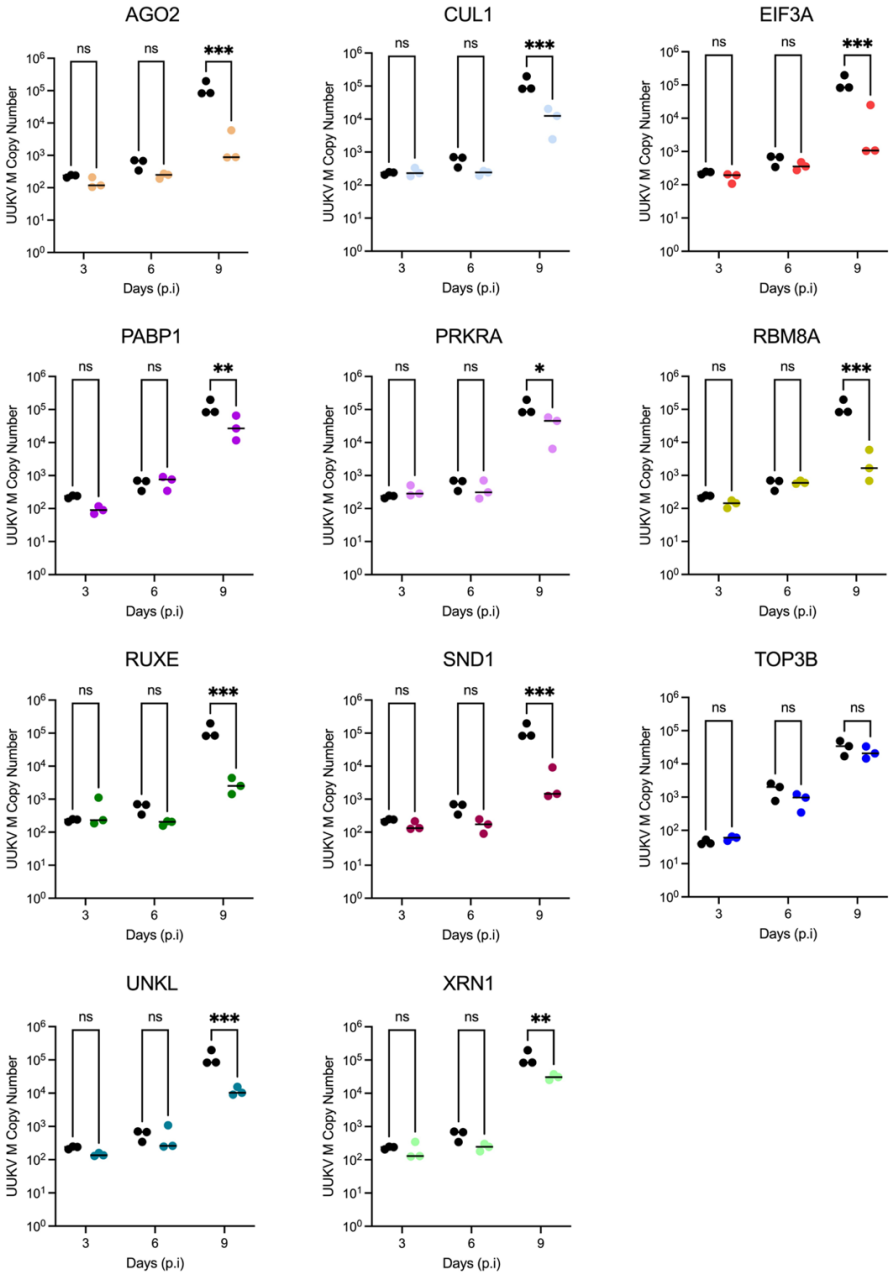

Fig 6. Effect of dsRNA transfections on quantity of UUKV M RNA present in rUUKV-infected ISE6 cell cultures.

Triplicate ISE6 cell monolayers were transfected with 2µg of dsRNA homologous to the indicated gene. Black symbols represent dseGFP data (mock) and coloured symbols represent dsGene data. At one day post-transfection, cell monolayers were infected with rUUKV at 5 FFU/cell. At timepoints indicated, cell supernatant was harvested, and UUKV M RNA copy number determined by RT-qPCR. Statistical significance was measured by ordinary two-way ANOVA with Tukey's multiple comparisons test. Asterisks indicates significance **** = $p < 0.0001$, *** = $p \leq 0.001$, ** = $p \leq 0.01$, * = $p \leq 0.05$, ns = not significant.

Another scientific advancement that has made the work described here possible is the methodology of exposing cell cultures to UV radiation to induce covalent crosslinking of RNA molecules to the proteins with which they interact (RNA-Interactome Capture).

This method has been successfully employed within many species, including humans [39], mice [40], fish (*Danio rerio*) [41], *Drosophila spp.* [42], parasites (*Leishmania spp.*) [43], yeast (*Saccharomyces cerevisiae*) [44], and plants (*Arabidopsis thaliana*) [45]. In collaboration with the Castello laboratory, the RNA-binding proteome of two mosquito species (*Aedes aegypti* and *Aedes albopictus*) and a tick species (*I. scapularis*) have now also been defined [manuscript in preparation]. This work allowed us to elucidate the RBPome of ISE6 cell cultures, but this was a snapshot of naïve cells and gave no information on what occurs during viral infection. In addition, it was unclear if this technique would be suitable for defining the RBPome of virus-infected tick cell lines.

In this manuscript we confirmed the use of the RIC methodology in rUUKV-infected ISE6 cell cultures and established a baseline methodology for investigating the effect of virus replication upon the infected tick cell (Fig 1). Despite bunyavirus mRNA molecules lack of a poly-A tail [33,34], the genome of UUKV contained sufficient poly-A like sequences to allow for mRNA capture without the necessity for a probe-based capture step in the methodology. Following the viral RIC within the cells, over 80% of human orthologs of the enriched proteins were shown to be RNA-binding proteins, and therefore we were confident this data would allow the characterisation of the first novel differentially active RBPome within rUUKV-infected tick cells (Fig 2). We identified 283 proteins whose RNA binding activity was significantly altered during infection. However, one caveat to this is that cannot determine if this differential binding activity is due to changes in the protein quantity within the cell or modulation of protein activity/function due to the lack of antibodies to tick proteins available, that would aid in visualisation of protein quantity.

Additionally, although this study focused on further investigation of several of the 156 targets that were found to have an increase in RNA binding activity during rUUKV infection, this does not mean that the downregulated proteins are not also important in viral infection. Routine vertebrate cell biology methodologies such as CRISPR/CAS9 [46] or protein overexpression from ectopically expressed plasmid vectors [47,48] have only very recently been applied to tick cell cultures. These novel techniques would allow for further future characterisation of the role of RBPs defined in this manuscript.

Through our UUKV N protein immunoprecipitation experiments we demonstrated that proteins within the differentially active RBPome can also interact with viral proteins (Fig 2). This is not unexpected as both the N and L proteins of bunyaviruses have been demonstrated to have a strong propensity to bind viral RNA [49,50]. The interaction of viral proteins with RBPs may be part of the mechanism to maximise potential interaction or activity with RNA, or a separate mechanism independent of RNA activity. Further future mutational analysis and protein modelling may be able to shed more light on these mechanisms, similar extensive mutagenesis studies have been conducted for other bunyaviruses [51].

Once the differential RBPome had been established we employed dsRNA knockdown delivered into the tick cells via a novel magnetofection methodology (Fig 3). Transient knockdown of tick cell genes had previously been demonstrated in a range of tick cell lines [52] and using this methodology we were able to achieve successful and sustained depletion of the target genes.

One of the main limitations of this and many other studies with tick cells are the lack of both genome annotation and molecular biology tools. To overcome these

limitations, we performed ortholog analysis of the identified proteins and protein domains within the differential RBPome and compared to the mammalian equivalents where possible. While this can and has been informative, data should be interpreted carefully as we can yet be certain that the identified tick proteins perform the same function as their mammalian counterparts.

The preliminary results gained from the dsRNA knockdown of selected targets confirm that these genes do impact the replication of UUKV in tick cells (Fig 4-6). One of the most interesting results was that found with the knockdown of *ISCI010954* (*TOP3B* in mammalian systems). TOP3B has already been demonstrated to have an impact on *Flavivirus* replication, but interestingly was not reported to affect the replication of two negative sense viruses in mammalian systems [36]. The suggested mechanism for this is that TOP3B aids in changing the conformation of the UUKV RNA to promote replication, transcription and/or translation. It is unclear if TOP3B is packaged into viral particles, however if this is the case it may be used to unwrap the UUKV RNA from the viral nucleocapsid to promote initial viral infection. While most topoisomerases bind DNA and have a nuclear subcellular localisation, under certain conditions, TOP3B can bind mRNAs associated with neuronal cell development in stress granules within the cytoplasmic compartment, the protein is also necessary for normal synapse formation in both *Drosophila* and mice [53]. Given the neuronal nature of the ISE6 cell line [54], and the similarity between viral replication factories and stress granules within the cytoplasm of infected cells, it is tempting to speculate that TOP3B is performing a similar function in the infected tick cell and hence impacting virus replication.

In this manuscript we have demonstrated the use of cRIC to interrogate the molecular interactions of a tickborne virus RNA genome with an arthropod cell. This work builds the foundation for our understanding of the importance of RNA-protein interactions during infection of arthropods and provides a starting point for further and more detailed characterisation of the hits identified in this novel differential RBPome. Ticks are important vectors of disease that can be infected for their entire lifespan. Obtaining a detailed picture how these viruses interact within the arthropod can only lead to a greater understanding of arbovirus transmission and accelerate research to counteract their spread.

ACKNOWLEDGEMENTS

We thank Prof. Ulrike Munderloh, University of Minnesota, for permission to use the ISE6 cell line.

FUNDING

This research was funded by the University of Glasgow MVLS DTP (A.W.) and a Wellcome Trust/Royal Society Sir Henry Dale Fellowship (210462/Z/18/Z) (B.B.). The facilities used in this study were funded by the UK Medical Research Council (MC_UU_00034/4, MC_UU_00034/7). L.B.S. is supported by the Wellcome Trust grant no. 223743/Z/21/Z. A.C. is funded by the European Research Council (ERC) Consolidator Grant ‘vRNP-capture’ 101001634 and the MRC grants MR/R021562/1 and MC_UU_00034/2. S.M., Y.D. and E.K. are funded by an EPSRC grant (V011359/1 (P). This research was funded in whole or in part by the Wellcome Trust. The funders

602 had no role in study design, data collection and analysis, decision to publish, or
603 preparation of the manuscript.
604
605 ## AUTHORS' CONTRIBUTIONS
606
607 Conceptualization: A.K., A.C., B.B.; Data Curation: A.W., W.K., D.L., Y.D., A.C., B.B.;
608 Formal Analysis: A.W., W.K., D.L., Y.D., M.N., S.M., A.C., B.B.; Funding Acquisition:
609 S.M., A.C., B.B.; Investigation: A.W., W.K., K.D., Y.D., M.N., Methodology: A.W., W.K.,
610 D.L., E.K., S.M., A.C., B.B.; Project administration: A.C., B.B.; Resources: A.W., W.K.,
611 K.D., L.B.S., M.N., S.M., A.C., B.B.; Supervision: A.K., S.M., A.C., B.B.; Validation:
612 A.W., W.K., A.C., B.B.; Visualization: A.W., W.K., A.C., B.B.; Writing – original draft:
613 A.W., W.K., A.C., B.B.; Writing – review & editing: A.W., W.K., K.D., L.B.S., D.L., Y.D.,
614 E.K., M.N., A.K., S.M., A.C., B.B.
615
616 ## DATA AVAILABILITY
617
618 The data that support the findings of this study are openly available from Enlighten
619 Research Data. Authors will make reagents described in this study available on
620 request (by qualified researchers for their own use). Requests should be directed to
621 the corresponding author.
622
623 ## MATERIALS AND METHODS

624 ### Experimental model and subject detail

625 **Cell culture**
626 Mammalian cell cultures used in this study were BSR and BSR-T7/5-CL21 (referred
627 to as BSR-T7) cells were provided by Karl-Klaus Conzelmann from the Ludwig-
628 Maximilians-Universität München. The BSR cell line is a clone of BHK-21 [55]. BSR-
629 T7 cell cultures are a modified BSR cell line stably transfected with the bacteriophage
630 T7 RNA polymerase [56]. Both cell lines were maintained in DMEM (Thermo Fisher
631 Scientific) supplemented with 10% (v/v) FBS at 37°C with 5% CO_2. BSR-T7 cell
632 medium was supplemented with 1mg/ml of the selection agent Geneticin (G418) prior
633 to transfection. The tick cell line used in this study was ISE6, derived from embryonic
634 *I. scapularis* [31], sourced from the Tick Cell Biobank at the University of Liverpool.
635 Cell lines were grown in flat-sided tubes (Nunc) for maintenance and transferred to
636 sealed T25 or T80 non-vented flasks for experimentation. ISE6 cells were maintained
637 at 32°C in enriched L-15B300 medium [57], supplemented with 10% tryptose
638 phosphate broth (TPB), 5% foetal bovine serum (FBS), 2 mM l-glutamine and 0.1%
639 bovine lipoprotein concentrate.
640
641 **Virus Production**
642 UUKV used in this project was a recombinant UUKV based derived from reverse
643 genetic technologies based upon the prototype tick isolate S-23 [3]. Working stocks of
644 UUKV were generated from recombinant virus rescue in BSR-T7 cells, followed by
645 generation of working stocks following amplification in BSR cell cultures. UUKV stocks
646 were titrated using an immunofocus assay.
647
648 **Immunofocus Assay**
649 Virus titres were enumerated by an immunofocus assay in BSR cells. Briefly, confluent
650 monolayers of BSR cells were infected with serial dilutions of virus made in phosphate

651 buffer saline (PBS) containing 2% FCS and incubated for 1h at 37 °C, followed by the
652 addition of a GMEM overlay supplemented with 2% FCS and 0.6% Avicel (FMC
653 Biopolymer). The cells were incubated for 5 days before fixation and subsequent use
654 of focus-forming assays as described previously [13, 32].
655

656 **RNA interactome capture (RIC)**

657 Comparative RNA interactome capture (RIC) was performed following a previously
658 described protocol by Castello et al, 2013 [58], with the following modifications. ISE6
659 cells were seeded in six sets of 3 x 10cm dishes with 1.5 x 10^7 cells/plate. Plates were
660 either mock-infected or inoculated with rUUKV at a multiplicity of infection (MOI) of 5
661 FFU/cell. Samples were harvested at 9 days p.i., when cell were washed 3x with PBS,
662 then irradiated with 150 mJ/cm^2 of UV light at 254nm on ice and lysed with 3ml of lysis
663 buffer (20mM Tris-HCl [pH 7.5], 500mM LiCl, 0.5% [w/v] LiDS, 1mM EDTA, 0.1% [v/v]
664 IGPAL, and 5mM DTT) per 3 plates. Lysates were then mechanically homogenised by
665 passing the sample through a 32G diameter needle using a 5ml syringe on ice. A
666 sample of homogenized lysate was removed at this stage for silver staining and qPCR
667 analysis. Oligo$(dT)_{25}$ capture beads were equilibrated in lysis buffer, and 300µl of the
668 vortexed bead slurry mix was added to each of the 6 samples and incubated for 1 hour
669 at 4°C with gentle rocking. Beads were collected in 1.5ml microcentrifuge tubes via a
670 magnet, and the lysates removed and discarded. Beads were then washed with lysis
671 buffer, wash buffer 1 (20mM Tris-HCl [pH 7.5], 500mM LiCl, 1mM EDTA, 0.01% [v/v]
672 IGEPAL, and 5mM DTT), wash buffer 2 (20mM Tris-HCl [pH 7.5], 500mM LiCl, 1mM
673 EDTA, 0.01% [v/v] IGPAL, and 5mM DTT) on ice, followed by wash buffer 3 (Oligo(dT)
674 buffer 3: 20mM Tris0HCl [pH 7.5], 200mM LiCl, 1mM EDTA, and 5mM DTT) at room
675 temperature. To wash, 1ml of the appropriate buffer was added to the beads. The
676 beads were inverted 10 times per minute, for five minutes, whilst being stored on ice
677 or at room temperature as specified. The beads were washed 3 times with each of the
678 buffers utilised in the protocol. Beads were resuspended in 125µl of elution buffer
679 (20mM Tris-HCl [pH 7.5] and 1mM EDTA) and incubated for 3 min at 55°C with
680 agitation. Finally, prepared eluates were stored at -80°C.
681

682 **Coimmunoprecipitation**

683 Coimmunoprecipitation (co-IP) was carried out using ISE6 cell monolayers infected
684 with rUUKV at a MOI of 5 FFU/cell, as described above. Mouse anti-UUKV N
685 antibodies, generated from hybridoma 8B11A3 (kindly provided by Dr Anna Overby)
686 were cross-linked to Dynabeads™ Protein G (Thermo Fisher) using BS3
687 (bis(sulfosuccinimidyl)suberate) following the manufacturer's instructions. Antibody
688 cross-linked beads were prepared for use in immunoprecipitation by washing in 500µl
689 of lysis buffer (20mM Tris, 150mM NaCl, 5mM MgCl2, 0.5% [v/v] NP40, 25 unit/ml
690 Benzonase (Merck Millipore), fresh cOmplete protease inhibitor [1 tablet per 10ml of
691 buffer], phosphatase inhibitor [Roche, 1 tablet per 10ml of buffer] per 100µl bead mix
692 with gentle rotation at 4°C for five minutes and finally stored in lysis buffer at 4°C.
693 At 9 days p.i., cells were lysed in 1ml of lysis buffer per plate. Cell lysates from either
694 mock or UUKV-infected triplicate plates were pooled and kept on ice.
695
696 Supernatants were clarified by centrifugation for 20 minutes and transferred to fresh
697 falcon tubes where 100µl of the lysates were removed for analysis by silver staining.

698 Prepared antibody-cross-linked beads were incubated with the cleared lysates and
699 incubated with gentle rotation at 4°C overnight. Beads were then collected using a
700 magnet, and supernatant discarded. Beads were washed with 500µl of wash buffer
701 (50mM Tris, 200mM NaCl, 1mM EDTA, 1% [v/v] NP40, fresh cOmplete protease
702 inhibitor [1 tablet per 10ml / buffer]) with gentle rotation at 4°C for five minutes.
703 Washing was repeated three times then the proteins eluted by incubation of the beads
704 with 125µl of elution buffer (100mM TEAB, 5% SDS [w/v]) at 95°C for 10 minutes.
705 Protein eluates were stored at -80°C prior to subsequent analysis.
706

707 **Synthesis of double stranded RNA (dsRNA).**

708 RNA was extracted from ISE6 cells using TRIzol, following the chloroform extraction
709 protocol by Invitrogen. Reverse transcription (RT) was carried out using the
710 SuperScript™ Reverse Transcriptase kit and random hexamers (50µM) to produce
711 cDNAs corresponding to cellular or viral targets (listed in Table S1). Unique portions
712 of the gene candidates were amplified from the prepared cDNAs with primers
713 incorporating a minimal T7 promoter sequence (All primer sequences can be found in
714 1). PCR products were analysed by agarose gel electrophoresis and purified by gel
715 extraction. PCR products were sequenced for target verification before the production
716 of dsRNA. The MEGAscript® RNAi Kit (Thermo Fisher Scientific) was used to produce
717 the dsRNA from the PCR fragments, according to the manufacturer's instructions. To
718 determine the quality of the dsRNA, the concentration was determined using the
719 Nanodrop One. Once prepared dsRNAs were stored at -80°C.
720

721 **dsRNA knockdown in tick cell cultures**

722 ISE6 cells were seeded into plates and monolayers were transfected using the
723 Magnetofectamine O2 transfection kit (1ug of dsRNA/1x10^6 cells), at the indicated
724 ratio of dsRNA:transfection reagent, 2µl of magnetofectamine beads, and 250µl
725 OptiMEM (Gibco), following manufacturers protocol (Oz Biosciences). After
726 transfection, transfections medium was removed, and fresh medium applied.
727 Monolayers were then incubated for 20 hours before infection with rUUKV at a MOI of
728 5 FFU/cell. Cell monolayers were harvested at the time points indicated and analysed
729 using RT qPCR, cell viability assays, whole cell immunofluorescent analysis, and foci-
730 forming assay to assess the production of infectious virus particles.
731

732 **Whole cell immunofluorescent analysis**

733 For immunofluorescent analysis in UUKV-infected cultures. Cell supernatant was
734 removed, and monolayers washed with PBS. Cells were fixed in 8% formaldehyde
735 solution for 1 hour and permeabilised in permeabilization buffer (0.5% [v/v] Triton X-
736 100 [Roth] in PBS) for 30 minutes. For both primary and secondary antibody buffers,
737 the corresponding antibodies (Mouse anti-UUKV generated from hybridoma 8B11A3
738 and Anti-mouse IgG (H&L) Secondary Invitrogen #T6199, respectively) were diluted
739 in blocking buffer (4% (w/v) semi-skimmed milk powder in PBST - 0.1% (v/v) tween
740 [Sigma] in PBS). The cell monolayers were then washed three times with PBS before
741 being probed with primary antibody buffer. Primary antibody incubation was carried
742 out overnight at 4°C. Cells were then washed three times with PBS before being
743 probed for 1 hour at room temperature with secondary antibody. Cells were washed
744 once with PBS before being incubated with DAPI diluted in PBS (3µl:10mL buffer) for

745 10 minutes at room temperature. Finally, cell monolayers were washed three times
746 with PBS. Cells were kept at 4°C in PBS until imaging. Monolayers were imaged using
747 an Odyssey® CLx Imaging System (Li-Cor) and analysed using the associated
748 software to determine the total UUKV N fluorescence compared to a mock-infected
749 well as a control.
750

751 **Cell viability assay**

752 CellTiter-Glo® 2.0 Cell Viability Assay (Promega) was used to determine the viability
753 of transfected cell monolayers. At the appropriate timepoint, cell monolayers were
754 washed before being resuspended in 150µl of fresh PBS. 50µl of the cell resuspension
755 or PBS control was pipetted into opaque-walled 94 well plates in triplicates. The cell
756 resuspension was then mixed with 50µl of viability reagent and incubated in the dark
757 for 10 minutes at room temperature. Well luminescence was measured using the
758 GloMax® Navigator Microplate Luminometer (Promega).
759

760 **Reverse-transcription and quantitative PCR**

761 RNA was isolated from cell monolayers or infected cell supernatant using TRIzol,
762 following the chloroform extraction protocol (Invitrogen). Reverse transcription (RT) to
763 generate cDNA was carried out using the SuperScript™ Reverse Transcriptase kit and
764 random hexamers (50µM; Thermo Fisher Scientific), following the manufacturer's
765 instructions. Positive controls were generated from randomly primed cDNA derived
766 from either total cell RNA or rUUKV-infected cell culture supernatant. For negative
767 controls, cDNA was replaced with nuclease-free H2O. qPCR primers for UUKV were
768 designed to target the genomic M RNA. qPCR analysis was undertaken using SYBR-
769 green (Applied Biosystems) on a QuantStudio 5 Real-Time PCR System (Applied
770 Biosystems) and associated software. Details of the primers used for qPCR in this
771 study can be found in Table S2. Transcript expression levels relative to the ISE6 18S
772 ribosomal subunit as a reference were calculated according to the $2^{-\Delta\Delta CT}$ methodology
773 [59]. Where no housekeeping gene present to allow for the ΔΔCt calculation, such as
774 when isolating UUKV M RNA from supernatant, Ct values were normalized, or a
775 standard curve was produced to allow gene copy number to be determined. The
776 maximum detection limit for the thermocycler was defined as a Ct of 40, and negative
777 controls produced a Ct of 30 or above. Therefore, any samples which produced a
778 normalised Ct ≤ 10 were therefore classified as a negative result.
779

780 **Conventional Protein Analysis**

781 If cells monolayers were not lysed through prior protocols, lysis of mock or rUUKV-
782 infected cell monolayers was carried out using Laemmli buffer. Samples were resolved
783 on SDS-PAGE and visualised via Pierce™ Silver Stain Kit (Thermo Fisher Scientific
784 #24612) and/or western blotting using mouse anti-UUKV N and anti-mouse IgG (H&L)
785 secondary, the Li-Cor Odyssey system for visualization and the Image Studio Lite
786 software (Li-Cor) for quantification. Data shown in the manuscript are representative
787 gels from at three independent replicates.
788

789 **Mass spectrometry and relative protein quantification**

790 RIC and NCAP pulldown eluates were processed through single-pot solid-phase-
791 enhanced (SP3) as previously described [36] and SDS-PAGE followed by in-gel

digestion sample preparation, respectively. ISE6 RIC and NCAP pulldown eluates prepared samples were sent to the Rosalind Franklin Institute and Dundee FingerPrints Proteomics facility respectively, for mass-spectrometry analysis (in data-dependent mode and label-free quantification), and the raw data files were provided upon completion. Protein identification and quantification were obtained using Andromeda search engine implemented in MaxQuant (v2.4.11.0) and searched against the ISE6 reference proteome [16] and UUKV proteome [8] with 'match between run' activated and under default parameters.
MaxQuant outputs (proteinGroups) were used for downstream relative quantification. Potential proteins contaminants flagged by MaxQuant were filtered out, R-package "DEP (1.4.1)", together with proteins with missing values across all samples. For relative quantification between UV-crosslinked versus non-crosslinked infected samples, proteins raw intensities were log2-transformed. Missing value imputation was performed only for proteins undetected in all replicates in one experimental condition, while present in the other condition (at least in 2 replicates). Imputation was implemented using minimum determination method (Mindet) [64]. Next, the processed protein intensities were subjected to statistical analysis using the empirical Bayesian method moderated t-test with p-values adjusted for multiple-testing (Benjamini-Hochberg method) provided by R-package "limma (3.38.3)" for. For all other comparisons, protein intensities were processed as described above with inclusion a normalization step of raw protein intensities using R-package Variance Stabilizing Normalization "VSN (3.50.0)".

Protein orthologs identification

To identify human (Uniprot_id: UP000005640, downloaded Nov2016) and fly (Uniprot_id: UP000000803, downloaded Aug2024) orthologs for ISE6 proteins InParanoid-DIAMOND was used under default settings [60,61].

Reactome enrichment analysis

Enrichment analysis of cellular pathways in differentially regulated RNA binding proteins was performed by R package ReactomePA. The analysis only included ISE6 proteins with human orthologs and all human genes as background [62].

Quantification and Statistical Analysis

For each condition, biological triplicates were produced, where each biological sample was tested (for example by RT qPCR) in triplicate, and an average of the technical replicates was then used for plotting and statistical analysis. Testing for statistical significance was carried out by either unpaired t-test, one-way ANOVA, or two-way ANOVA with Tukey's multiple comparison. The cut-off for significance was set at $p<0.05$. Where analysis was employed, unless stated otherwise both "ns" and a lack of notation indicate no significance.

REFERENCES

1. Oker-Blom N., Salminen A., Brummer-Korvenkontio M., Kaeaeriaeinen L., Weckstroem P. (1964) Isolation of some viruses other than typical tick-borne encephalitis viruses from Ixodes ricinus ticks in Finland. Ann Med Exp Biol Fenn 42: 109-112.

2. Mazelier M., Rouxel R. N., Zumstein M., Mancini R., Bell-Sakyi L., Lozach P. Y. (2016) Uukuniemi Virus as a Tick-Borne Virus Model. J Virol 90: 6784-6798.
3. Rezelj V. V., Överby A. K., Elliott R. M. (2015) Generation of mutant Uukuniemi viruses lacking the nonstructural protein NSs by reverse genetics indicates that NSs is a weak interferon antagonist. J Virol 89: 4849-4856.
4. Pettersson R. F., Hewlett M. J., Baltimore D., Coffin J. M. (1977) The genome of Uukuniemi virus consists of three unique RNA segments. Cell 11: 51-63.
5. Ranki M., Pettersson R. F. (1975) Uukuniemi virus contains an RNA polymerase. J Virol 16: 1420-1425.
6. Overby A. K., Pettersson R. F., Grünewald K., Huiskonen J. T. (2008) Insights into bunyavirus architecture from electron cryotomography of Uukuniemi virus. Proc Natl Acad Sci U S A 105: 2375-2379.
7. Lozach P. Y., Kühbacher A., Meier R., Mancini R., Bitto D., Bouloy M., Helenius A. (2011) DC-SIGN as a receptor for phleboviruses. Cell Host Microbe 10: 75-88.
8. Lozach P. Y., Mancini R., Bitto D., Meier R., Oestereich L., Overby A. K., Pettersson R. F., Helenius A. (2010) Entry of bunyaviruses into mammalian cells. Cell Host Microbe 7: 488-499.
9. Meier R., Franceschini A., Horvath P., Tetard M., Mancini R., von Mering C., Helenius A., Lozach P. Y. (2014) Genome-wide small interfering RNA screens reveal VAMP3 as a novel host factor required for Uukuniemi virus late penetration. J Virol 88: 8565-8578.
10. Elliott R. M., Brennan B. (2014) Emerging phleboviruses. Curr Opin Virol 5: 50-57.
11. Rezelj V. V., Li P., Chaudhary V., Elliott R. M., Jin D. Y., Brennan B. (2017) Differential Antagonism of Human Innate Immune Responses by Tick-Borne Phlebovirus Nonstructural Proteins. mSphere 2.
12. Palacios G., Savji N., Travassos da Rosa A., Guzman H., Yu X., Desai A., Rosen G. E., Hutchison S., Lipkin W. I., Tesh R. (2013) Characterization of the Uukuniemi virus group (Phlebovirus: Bunyaviridae): evidence for seven distinct species. J Virol 87: 3187-3195.
13. Salata C., Moutailler S., Attoui H., Zweygarth E., Decker L., Bell-Sakyi L. (2021) How relevant are in vitro culture models for study of tick-pathogen interactions? Pathog Glob Health 115: 437-455.
14. Jia N., Wang J., Shi W., Du L., Sun Y., et al. (2020) Large-Scale Comparative Analyses of Tick Genomes Elucidate Their Genetic Diversity and Vector Capacities. Cell 182: 1328-1340.e1313.
15. Gulia-Nuss M., Nuss A. B., Meyer J. M., Sonenshine D. E., Roe R. M., et al. (2016) Genomic insights into the Ixodes scapularis tick vector of Lyme disease. Nat Commun 7: 10507.
16. Miller J. R., Koren S., Dilley K. A., Harkins D. M., Stockwell T. B., Shabman R. S., Sutton G. G. (2018) A draft genome sequence for the Ixodes scapularis cell line, ISE6. F1000Res 7: 297.
17. Bell-Sakyi L., Zweygarth E., Blouin E. F., Gould E. A., Jongejan F. (2007) Tick cell lines: tools for tick and tick-borne disease research. Trends Parasitol 23: 450-457.
18. Schnettler E., Tykalová H., Watson M., Sharma M., Sterken M. G., Obbard D. J., Lewis S. H., McFarlane M., Bell-Sakyi L., Barry G., Weisheit S., Best S. M., Kuhn R. J., Pijlman G. P., Chase-Topping M. E., Gould E. A., Grubhoffer L., Fazakerley J. K., Kohl A. (2014) Induction and suppression of tick cell antiviral RNAi responses by tick-borne flaviviruses. Nucleic Acids Res 42: 9436-9446.
19. Weisheit S., Villar M., Tykalová H., Popara M., Loecherbach J., Watson M., Růžek D., Grubhoffer L., de la Fuente J., Fazakerley J. K., Bell-Sakyi L. (2015) Ixodes

890 scapularis and Ixodes ricinus tick cell lines respond to infection with tick-borne
891 encephalitis virus: transcriptomic and proteomic analysis. Parasit Vectors 8: 599.
892 20. Grabowski J. M., Gulia-Nuss M., Kuhn R. J., Hill C. A. (2017) RNAi reveals proteins
893 for metabolism and protein processing associated with Langat virus infection in Ixodes
894 scapularis (black-legged tick) ISE6 cells. Parasit Vectors 10: 24.
895 21. McNally K. L., Mitzel D. N., Anderson J. M., Ribeiro J. M., Valenzuela J. G., Myers
896 T. G., Godinez A., Wolfinbarger J. B., Best S. M., Bloom M. E. (2012) Differential
897 salivary gland transcript expression profile in Ixodes scapularis nymphs upon feeding
898 or flavivirus infection. Ticks Tick Borne Dis 3: 18-26.
899 22. Mansfield K. L., Cook C., Ellis R. J., Bell-Sakyi L., Johnson N., Alberdi P., de la
900 Fuente J., Fooks A. R. (2017) Tick-borne pathogens induce differential expression of
901 genes promoting cell survival and host resistance in Ixodes ricinus cells. Parasit
902 Vectors 10: 81.
903 23. Simser J. A., Macaluso K. R., Mulenga A., Azad A. F. (2004) Immune-responsive
904 lysozymes from hemocytes of the American dog tick, Dermacentor variabilis and an
905 embryonic cell line of the Rocky Mountain wood tick, D. andersoni. Insect Biochem
906 Mol Biol 34: 1235-1246.
907 24. Sidak-Loftis L. C., Rosche K. L., Pence N., Ujczo J. K., Hurtado J., Fisk E. A.,
908 Goodman A. G., Noh S. M., Peters J. W., Shaw D. K. (2022) The Unfolded-Protein
909 Response Triggers the Arthropod Immune Deficiency Pathway. mBio 13: e0070322.
910 25. Uckeley Z. M., Moeller R., Kühn L. I., Nilsson E., Robens C., Lasswitz L., Lindqvist
911 R., Lenman A., Passos V., Voss Y., Sommerauer C., Kampmann M., Goffinet C.,
912 Meissner F., Överby A. K., Lozach P. Y., Gerold G. (2019) Quantitative Proteomics of
913 Uukuniemi Virus-host Cell Interactions Reveals GBF1 as Proviral Host Factor for
914 Phleboviruses. Mol Cell Proteomics 18: 2401-2417.
915 26. Castello A., Iselin L. (2023) Viral RNA Is a Hub for Critical Host-Virus Interactions.
916 Subcell Biochem 106: 365-385.
917 27. Bermudez Y., Hatfield D., Muller M. (2024) A Balancing Act: The Viral-Host Battle
918 over RNA Binding Proteins. Viruses 16.
919 28. Garcia-Moreno M., Noerenberg M., Ni S., Järvelin A. I., González-Almela E., et al.
920 (2019) System-wide Profiling of RNA-Binding Proteins Uncovers Key Regulators of
921 Virus Infection. Mol Cell 74: 196-211.e111.
922 29. Kamel W., Noerenberg M., Cerikan B., Chen H., Järvelin A. I., et al. (2021) Global
923 analysis of protein-RNA interactions in SARS-CoV-2-infected cells reveals key
924 regulators of infection. Mol Cell 81: 2851-2867.e2857.
925 30. Lisy S., Rothamel K., Ascano M. (2021) RNA Binding Proteins as Pioneer
926 Determinants of Infection: Protective, Proviral, or Both? Viruses 13.
927 31. Kurtti T. J., Munderloh U. G., Andreadis T. G., Magnarelli L. A., Mather T. N. (1996)
928 Tick cell culture isolation of an intracellular prokaryote from the tick Ixodes scapularis.
929 J Invertebr Pathol 67: 318-321.
930 32. Iselin L., Palmalux N., Kamel W., Simmonds P., Mohammed S., Castello A. (2022)
931 Uncovering viral RNA-host cell interactions on a proteome-wide scale. Trends
932 Biochem Sci 47: 23-38.
933 33. Blakqori G., van Knippenberg I., Elliott R. M. (2009) Bunyamwera orthobunyavirus
934 S-segment untranslated regions mediate poly(A) tail-independent translation. J Virol
935 83: 3637-3646.
936 34. Bouloy M., Pardigon N., Vialat P., Gerbaud S., Girard M. (1990) Characterization
937 of the 5' and 3' ends of viral messenger RNAs isolated from BHK21 cells infected with
938 Germiston virus (Bunyavirus). Virology 175: 50-58.

35. Petit M., Flory C., Gu Q., Fares M., Davies K., Score A., Lamont D., Sakyi L. B.-., Scaturro P., Brennan B., Kohl A. (2024) Multi-omics analysis of severe fever with thrombocytopenia syndrome virus infection in Rhipicephalus microplus cells reveals antiviral tick factors. PREPRINT (Version 1) available at Research Square.
36. Diosa-Toro M., Prasanth K. R., Bradrick S. S., Garcia Blanco M. A. (2020) Role of RNA-binding proteins during the late stages of Flavivirus replication cycle. Virol J 17: 60.
37. Bell-Sakyi L., Hartley C. S., Khoo J. J., Forth J. H., Palomar A. M., Makepeace B. L. (2022) New Cell Lines Derived from European Tick Species. Microorganisms 10.
38. De S., Kingan S. B., Kitsou C., Portik D. M., Foor S. D., Frederick J. C., Rana V. S., Paulat N. S., Ray D. A., Wang Y., Glenn T. C., Pal U. (2023) A high-quality Ixodes scapularis genome advances tick science. Nature Genetics 55: 301-311.
39. Castello A., Fischer B., Eichelbaum K., Horos R., Beckmann B. M., Strein C., Davey N. E., Humphreys D. T., Preiss T., Steinmetz L. M., Krijgsveld J., Hentze M. W. (2012) Insights into RNA biology from an atlas of mammalian mRNA-binding proteins. Cell 149: 1393-1406.
40. Kwon S. C., Yi H., Eichelbaum K., Föhr S., Fischer B., You K. T., Castello A., Krijgsveld J., Hentze M. W., Kim V. N. (2013) The RNA-binding protein repertoire of embryonic stem cells. Nat Struct Mol Biol 20: 1122-1130.
41. Despic V., Dejung M., Gu M., Krishnan J., Zhang J., Herzel L., Straube K., Gerstein M. B., Butter F., Neugebauer K. M. (2017) Dynamic RNA-protein interactions underlie the zebrafish maternal-to-zygotic transition. Genome Res 27: 1184-1194.
42. Sysoev V. O., Fischer B., Frese C. K., Gupta I., Krijgsveld J., Hentze M. W., Castello A., Ephrussi A. (2016) Global changes of the RNA-bound proteome during the maternal-to-zygotic transition in Drosophila. Nat Commun 7: 12128.
43. Nandan D., Thomas S. A., Nguyen A., Moon K. M., Foster L. J., Reiner N. E. (2017) Comprehensive Identification of mRNA-Binding Proteins of Leishmania donovani by Interactome Capture. PLoS One 12: e0170068.
44. Tsvetanova N. G., Klass D. M., Salzman J., Brown P. O. (2010) Proteome-wide search reveals unexpected RNA-binding proteins in Saccharomyces cerevisiae. PLoS One 5.
45. Marondedze C., Thomas L., Serrano N. L., Lilley K. S., Gehring C. (2016) The RNA-binding protein repertoire of Arabidopsis thaliana. Sci Rep 6: 29766.
46. Sharma A., Pham M. N., Reyes J. B., Chana R., Yim W. C., Heu C. C., Kim D., Chaverra-Rodriguez D., Rasgon J. L., Harrell R. A., Nuss A. B., Gulia-Nuss M. (2022) Cas9-mediated gene editing in the black-legged tick, Ixodes scapularis, by embryo injection and ReMOT Control. iScience 25: 103781.
47. Singh N., Rolandelli A., O'Neal Anya J., Butler L. R., Samaddar S., Laukaitis-Yousey Hanna J., Butnaru M., Mohr Stephanie E., Perrimon N., Pedra Joao H. F. (2024) Genetic manipulation of an Ixodes scapularis cell line. mBio 15: e02479-02423.
48. Shi J., Zhou M., Tang S., Wu Q., Deng F., Bell-Sakyi L., Shen S. (2022) Differential characteristics of mammalian and tick-derived promoters to trigger protein expression in transfected tick cell lines. Ticks Tick Borne Dis 13: 101906.
49. Katz A., Freiberg A. N., Backström V., Schulz A. R., Mateos A., Holm L., Pettersson R. F., Vaheri A., Flick R., Plyusnin A. (2010) Oligomerization of Uukuniemi virus nucleocapsid protein. Virol J 7: 187.
50. Reguera J., Weber F., Cusack S. (2010) Bunyaviridae RNA polymerases (L-protein) have an N-terminal, influenza-like endonuclease domain, essential for viral cap-dependent transcription. PLoS Pathog 6: e1001101.

988 51. Eifan S. A., Elliott R. M. (2009) Mutational analysis of the Bunyamwera
989 orthobunyavirus nucleocapsid protein gene. J Virol 83: 11307-11317.
990 52. Barry G., Alberdi P., Schnettler E., Weisheit S., Kohl A., Fazakerley J. K., Bell-
991 Sakyi L. (2013) Gene silencing in tick cell lines using small interfering or long double-
992 stranded RNA. Exp Appl Acarol 59: 319-338.
993 53. Xu D., Shen W., Guo R., Xue Y., Peng W., et al. (2013) Top3beta is an RNA
994 topoisomerase that works with fragile X syndrome protein to promote synapse
995 formation. Nat Neurosci 16: 1238-1247.
996 54. Oliver J. D., Chavez A. S., Felsheim R. F., Kurtti T. J., Munderloh U. G. (2015) An
997 Ixodes scapularis cell line with a predominantly neuron-like phenotype. Exp Appl
998 Acarol 66: 427-442.
999 55. Sato M., Maeda N., Yoshida H., Urade M., Saito S., Miyazaki T., Shibata T.,
1000 Watanabe M. (1977) Plaque formation of herpes virus hominis type 2 and rubella virus
1001 in variants isolated from the colonies of BHK21/WI-2 cells formed in soft agar. Archives
1002 of Virology 53: 269-273.
1003 56. Buchholz U. J., Finke S., Conzelmann K. K. (1999) Generation of bovine
1004 respiratory syncytial virus (BRSV) from cDNA: BRSV NS2 is not essential for virus
1005 replication in tissue culture, and the human RSV leader region acts as a functional
1006 BRSV genome promoter. J Virol 73: 251-259.
1007 57. Munderloh U. G., Jauron S. D., Fingerle V., Leitritz L., Hayes S. F., Hautman J. M.,
1008 Nelson C. M., Huberty B. W., Kurtti T. J., Ahlstrand G. G., Greig B., Mellencamp M. A.,
1009 Goodman J. L. (1999) Invasion and intracellular development of the human
1010 granulocytic ehrlichiosis agent in tick cell culture. J Clin Microbiol 37: 2518-2524.
1011 58. Castello A., Horos R., Strein C., Fischer B., Eichelbaum K., Steinmetz L. M.,
1012 Krijgsveld J., Hentze M. W. (2013) System-wide identification of RNA-binding proteins
1013 by interactome capture. Nat Protoc 8: 491-500.
1014 59. Livak K. J., Schmittgen T. D. (2001) Analysis of relative gene expression data using
1015 real-time quantitative PCR and the 2(-Delta Delta C(T)) Method. Methods 25: 402-408.
1016 60. Perez-Perri J. I., Noerenberg M., Kamel W., Lenz C. E., Mohammed S., Hentze M.
1017 W., Castello A. (2021) Global analysis of RNA-binding protein dynamics by
1018 comparative and enhanced RNA interactome capture. Nat Protoc 16: 27-60.
1019 61. Persson E., Sonnhammer E. L. L. (2022) InParanoid-DIAMOND: faster orthology
1020 analysis with the InParanoid algorithm. Bioinformatics 38: 2918-2919.
1021 62. Yu G., He Q.-Y. (2016) ReactomePA: an R/Bioconductor package for reactome
1022 pathway analysis and visualization. Molecular BioSystems 12: 477-479.